Slc13a5 Expression in Ameloblast-Like Cells and Tooth Organ Cultures: A Platform for Therapeutic Studies

by

Kuan Yu Chu

A dissertation submitted in partial fulfillment
of the requirements for the degree of
Master of Science
(Oral Health Science)
in the University of Michigan
2026

Advisor:

Professor Jan C-C Hu
Professor Junichi Iwata
Associate Professor Shih-Kai Wang, National Taiwan University

Kuan Yu Chu

kychu@umich.edu

© Kuan Yu Chu 2026

Acknowledgements

I would like to express my sincere gratitude to Prof. Jan C.-C. Hu, Prof. Junichi Iwata, and Associate Prof. Shih-Kai Wang for their invaluable mentorship and guidance throughout this study. I am also deeply grateful to Associate Prof. Elizabeth Van Tubergen, Director of the OHS Master's Program, for her continuous support.

I would further like to acknowledge Dr. Ravi Prakash for assistance with cell culture and immunocytochemistry experiments, Dr. Hong Zhang for designing the RT-PCR primers and supporting the RT-PCR analyses, and Dr. Akiko Suzuki for guidance with histological procedures. In addition, I thank Dr. Chuhua Zhang for managing the mouse colony and generating the images presented in Figure 2, Dr. Yuanyuan Hu for producing the images used in Figures 3 and 4, and Dr. Tian Liang for generating Figure 5 while working in Dr. James Simmer's laboratory.

This study was supported by the National Institute of Dental and Craniofacial Research (NIDCR) under grant number UG3/UH3 DE028849.

Table of Contents

Acknowledgements ..... **iii**

List of Figures ..... **v**

Abstract ..... **vi**

Introduction **1**

Materials and Methods **6**

Cell Culture and Plasmid Transfection 6

Transcript Analyses 6

Immunocytochemistry 7

Tooth Organ Culture 7

Results **8**

Cell morphology and GFP reporter expression 8

Transcript Analyses 9

Immunocytochemistry 9

Tooth Organ Culture 10

Discussion **12**

Bibliography **15**

List of Figures

Figure 1: Severe hypoplastic enamel in an individual with SLC13A5 biallelic premature stop codon (p.Arg333*) mutation. 2

Figure 2: Hypoplastic enamel defect with severe attrition in Slc13a5$^{R337*/R337*}$ mice. 2

Figure 3: bSEM micrographs of 7-week mandibular incisors. 3

Figure 4: Knoop hardness testing of 7-week mandibular incisors at the level of enamel maturation. 3

Figure 6: *Slc13a5* overexpression in LS8 cells following plasmid transfection. 8

Figure 7: Immunocytochemical detection of Slc13a5 expression in LS8 cells. 10

Figure 8: Tooth organ culture of mandibular molars. 11

Abstract

Mutations in *SLC13A5*, encoding the sodium-dependent citrate transporter (NaCT), cause developmental and epileptic encephalopathy 25 (DEE25), a disorder characterized by severe neurological impairment and enamel defects, including hypoplastic amelogenesis imperfecta. Although the neurological features of DEE25 are well documented, the mechanisms underlying enamel abnormalities remain poorly understood. In this study, we established *in vitro* and *ex vivo* systems to investigate NaCT function in enamel development and to support future gene therapy approaches.

Mouse ameloblast-like LS8 cells were transfected with *Slc13a5* expression plasmids to evaluate transfection efficiency, as well as gene and protein expression. Transient overexpression of *Slc13a5* resulted in increased mRNA levels and detectable NaCT protein, with peak transcript expression at 48 hours and maximal protein and GFP reporter signal at 72 hours post-transfection. Immunocytochemistry further confirmed successful NaCT expression.

To model enamel defects *ex vivo*, tooth organ cultures were established from wild-type and *Slc13a5*$^{R337*/R337*}$ mouse molars. Mutant tooth germs in culture reproduced key pathological features observed *in vivo*, including irregular, ectopic mineral deposition. These findings demonstrate that the organ culture system can partially recapitulate the *in vivo* phenotype and serve as a platform for evaluating short-term gene delivery efficiency.

Together, these results validate LS8 cells and tooth organ cultures as complementary platforms for studying *Slc13a5* function and optimizing gene delivery strategies. This work provides a foundational step toward the development of adeno-associated virus (AAV)-based therapeutic approaches aimed at mitigating NaCT function and improving enamel defects associated with DEE25.

Introduction

SLC13A5 encodes the sodium-dependent citrate transporter (NaCT), which is primarily expressed in soft (liver, testes, brain) and hard (bone, teeth) tissues. NaCT functions as a dimer and is essential for cellular citrate uptake and metabolism[1, 2]. Citrate serves as a key intermediate in energy production, lipogenesis, inhibition of glycolysis, blood clotting, and pH regulation[3]. In addition, citrate contributes to the stabilization of hydroxyapatite nanocrystals in mineralized tissues such as bone and teeth[4]. Approximately 1.6% of bone content is citrate, and nearly 80% of total body citrate is stored in bone[5]. Mutations in *SLC13A5* cause autosomal recessive developmental and epileptic encephalopathy 25 (DEE25, MIM#615905), a rare but severe disorder characterized by neonatal-onset epilepsy, motor impairment, and cognitive dysfunction[6]. In addition to neurologic manifestations, patients with DEE25 present with dental abnormalities, including enamel hypoplasia, delayed tooth eruption, and abnormal dentin structure[7-9].

Enamel is the hardest and most highly mineralized tissue in the human body. It protects teeth from mechanical forces, chemical damages, temperature changes, and bacterial biofilm. Unlike many other tissues, enamel cannot regenerate after eruption because ameloblasts degenerate once tooth formation is complete. Amelogenesis imperfecta (AI) is a rare inherited disorder of enamel malformation. It can cause chronic pain, hypersensitivity, impaired mastication, speech difficulties, esthetic concerns, and reduced self-esteem. The reported prevalence ranges from 1 in 700 to 1 in 14,000[7]. Some mutations affecting amelogenesis also involve other organs, resulting in syndromic forms of AI[10].

Amelogenesis is a tightly regulated process. Both genetic and environmental disturbances can disrupt enamel formation. More than 115 genes and associated conditions have been linked to abnormal amelogenesis, including genes encoding enamel matrix proteins such as *AMELX*, processing proteases, *KLK4*, and proteins involved in hydroxyapatite crystallization such as *ODAPH*[10]. NaCT represents a membrane transporter that plays a critical role not only in the nervous system but also in enamel development. In mouse models, *Slc13a5* expression has been detected in ameloblasts, odontoblasts, and osteoblasts. In ameloblasts, NaCT localizes to both

proximal and distal membranes during the secretary and maturation stages, where it helps maintain citrate and energy homeostasis during enamel formation[11].

Individuals carrying biallelic premature stop mutations in *SLC13A5* (p.Arg333*) exhibit severe hypoplastic enamel (Fig.1). A *Slc13a5*$^{R337*/R337*}$ mouse model, homologous to the human *SLC13A5* $^{R333*/R333*}$ variant, has been established and presents a hypoplastic AI phenotype.



Figure 1: Severe hypoplastic enamel in an individual with SLC13A5 biallelic premature stop codon (p.Arg333*) mutation (Adopted from Figure 2 in Schossig et al., 2017).

At 7 weeks of age, *Slc13a5*$^{R337*/R337*}$ mice exhibit chalky white incisors and occlusally flattened molars, whereas no morphological differences are observed between wild type and *Slc13a5*$^{+/R337*}$ teeth (Fig.2). Backscattered scanning electron (bSEM) micrographs of mandibular incisors revealed enlarged dentinal tubules. Instead of forming a normal enamel layer, ectopic mineralized nodules deposit on the labial surface of dentin (Fig.3). Knoop hardness testing demonstrates that these nodules are significantly softer than normal enamel (Fig.4).

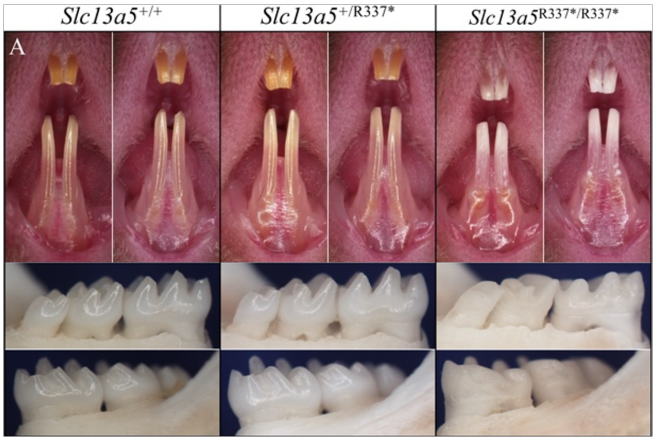


Figure 2: Hypoplastic enamel defect with severe attrition in Slc13a5$^{R337*/R337*}$ mice.

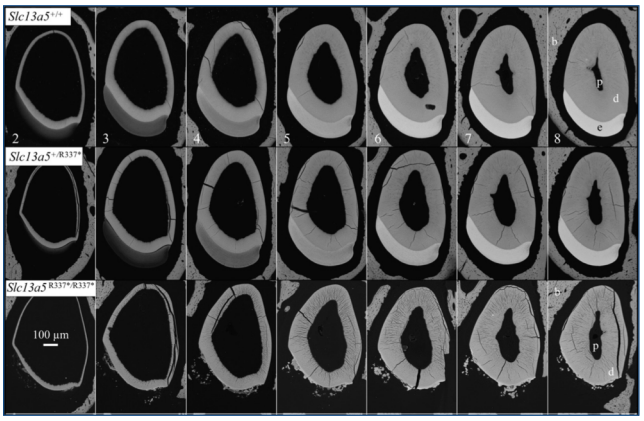


Figure 3: bSEM micrographs of 7-week mandibular incisors cross-sectioned at 1 mm increments.

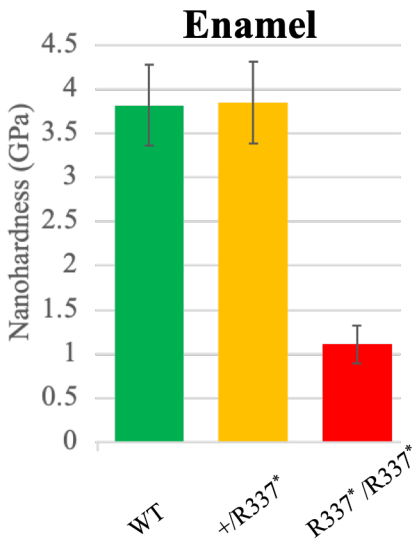


Figure 4: Knoop hardness testing of 7-week mandibular incisors at the level of enamel maturation.

The hypoplastic enamel phenotype is consistent with histologic findings. On postnatal day 12, *Slc13a5*$^{R337*/R337*}$ mice show dysplastic ameloblasts detached from the dentin surface and no appreciable enamel layer. Instead, ectopic calcified nodules accumulate on molar cusps and slopes, as well as on the labial surface of mandibular incisors (Fig.5).

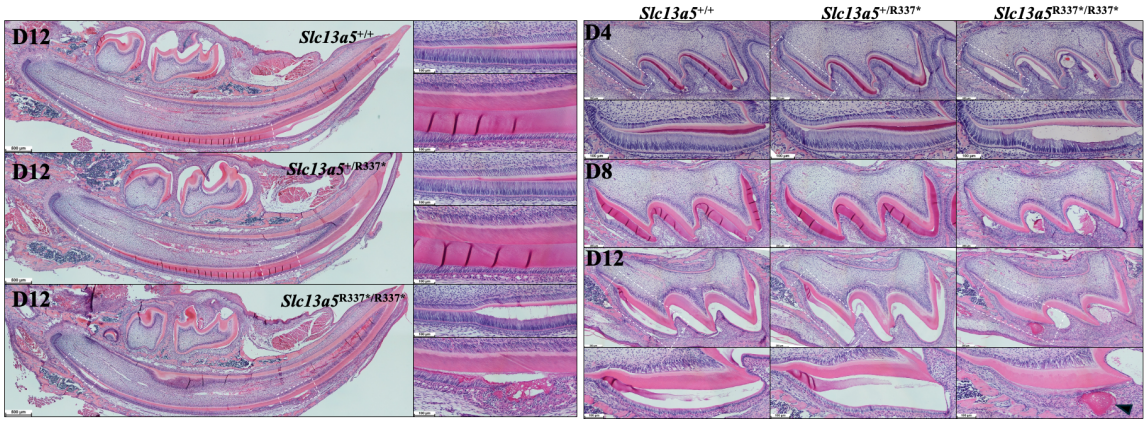


Figure 5: Morphologic and Histologic Evaluation of *Slc13a5*$^{+/+}$, *Slc13a5*$^{+/R337*}$, and *Slc13a5* $^{R337*/R337*}$ mouse mandibular incisors and maxillary molars. Histological analysis of D12 mandibular incisors in *Slc13a5*$^{R337*/R337*}$ mice exhibited hypoplastic enamel. No apparent differences were observed between *Slc13a5*$^{+/+}$ and *Slc13a5*$^{+/R337*}$ mouse incisors. D4, D8, and D12 maxillary molars revealed disturbed enamel matrix deposition during the early secretory stage and ectopic calcification during the maturation stage in *Slc13a5*$^{R337*/R337*}$ mice. Notably, no enamel matrix deposition was observed in *Slc13a5*$^{R337*/R337*}$ molars.

Although AI cases involving *SLC13A5* variants have been reported and the genetic mechanisms underlying enamel defects are increasingly understood, no effective therapies currently target the root genetic causes. The *Slc13a5*$^{R337*/R337*}$ mouse model serves as a valuable platform for elucidating the pathophysiological mechanisms underlying enamel hypoplasia resulting from the absence of NaCT. Additionally, it offers a stable system for evaluating therapeutic strategies aimed at improving outcomes for patients with DEE25. We hypothesized that *Slc13a5* constructs can be validated in mouse immortalized ameloblast-like cells (LS8 cells) using plasmid-based gene delivery, and that tooth organ cultures derived from *Slc13a5*$^{R337*/R337*}$ mice can reproduce key enamel abnormalities for gene delivery and expression studies. Our long-term goal is to establish a foundation for future therapeutic investigation using adeno-associated virus (AAV) constructs carrying the correct *Slc13a5* coding sequence delivered into developing *Slc13a5*$^{R337*/R337*}$ mouse molars *in vitro* to evaluate infection efficiency and gene expression levels.

To achieve this objective, we first assessed expression of pCMV constructs in LS8 cells to optimize experimental conditions. LS8 cells were transfected with *Slc13a5* plasmids to evaluate transfection efficiency, post-transfection cell viability, and duration of p*Slc13a5* overexpression. We also established tooth organ cultures to assess tissue viability, developmental progression, and mineralization patterns. Tooth germs can be dissected from newborn mice and

cultured *ex vivo*, enabling investigation of amelogenesis at defined developmental stages[12]. This *ex vivo* model is suitable for studying *Slc13a5* disfunction because it allows direct delivery of reagents into developing teeth germs while preserving three-dimensional structure and epithelial-mesenchymal interactions[13]. This pilot study represents the first step in evaluating the feasibility of gene expression studies in the *Slc13a5*$^{R337*/R337*}$ tooth organs and mouse model.

Materials and Methods

Cell Culture and Plasmid Transfection

LS8 mouse ameloblast-like cells were cultured in Dulbecco's Modified Eagle Medium (DMEM) supplemented with 10% fetal bovine serum (FBS) and 1% penicillin–streptomycin at 37 °C in a humidified atmosphere containing 5% CO_2. For transfection, 2.5×10^5 cells (12-well plates) or 5×10^5 cells (6-well plates) were seeded per well and transfected at 70–90% confluency. Cells were transfected with 1.5 µg DNA per well (12-well plates) or 2.5 µg DNA per well (6-well plates) of the *Slc13a5* expression plasmid using Lipofectamine™ 3000 (Thermo Fisher Scientific), according to the manufacturer's instructions. Cells were maintained under standard culture conditions until analysis. Cell morphology and GFP reporter expression were assessed at 48, 72, and 96 h post-transfection using an EVOS™ M7000 Imaging System (Thermo Fisher Scientific).

Transcript Analyses

Cells were harvested 48 h, 72 h, and 96 h after transfection. Total RNA was extracted using the RNeasy Mini Kit (Qiagen), and equal amounts of RNA were used for cDNA synthesis with the SuperScript™ III First-Strand Synthesis System (Invitrogen). PCR reactions (20 µL) consisted of 10 µL Platinum™ Hot Start PCR Master Mix (2×; Invitrogen), 1 µL of 10 µM primer sets, 1 µL cDNA template, and nuclease-free water. To detect the transcripts of *Slc13a5,* primer sets *Slc13a5*-F: 5'- CCAGACTGAGGAAGAAAGGAAA-3' and *Slc13a5*-R: 5'- TCCAAGTTAAACATAGCCCGA-3' covering exons 8 to 11 of TV1 producing an amplicon of 522 bp were used. Primer set to amplify *Gapdh* F: 5'- AGGCCGGTGCTGAGTATGTC-3' and *Gapdh* R: 5'- TGCCTGCTTCACCACCTTCT-3' producing an amplicon of 530 bp was used as experimental control. PCR was performed on a GeneAmp PCR System 9700 thermocycler using the following conditions: 94 °C for 2 min; 30 cycles of 94 °C for 30 s (template denaturation), 59 °C for 30 s (primer annealing), and 72 °C for 50 s (primer extension); followed by 72 °C for 2

min and a 4 °C hold. PCR products were separated on a 2% agarose gel through electrophoresis and imaged using a FluorChem M Imaging System (Bio-Techne, San Jose, California).

Immunocytochemistry

Cells were harvested 72 h after transfection and washed with PBS, fixed in 4% paraformaldehyde for 15 min, and permeabilized with 0.1% Triton X-100 for 10 min. Blocking was performed with 20% normal goat serum (NGS) for 2 h at room temperature. Cells were incubated with rabbit anti-NaCT primary antibody (Invitrogen; 1:100 in 2% NGS) for 1 h at room temperature followed by overnight incubation at 4 °C. After washing with PBS containing 0.25% Tween-20 (PBST) and PBS, cells were incubated with goat anti-rabbit Alexa Fluor Plus 594 secondary antibody (Invitrogen; 1:1500 in 2% NGS) for 1 h in the dark. Coverslips were mounted with DAPI-containing mounting medium (Abcam) and imaged using a Nikon A1R confocal microscope (Nikon, Melville, New York).

Tooth Organ Culture

Newborn (postnatal day 0) C57BL/6 wild-type and *Slc13a5*$^{R337*/R337*}$ mouse pups were decapitated followed by surface disinfection with 70% ethanol. The maxilla and mandible were separated, rinsed with PBS, and then placed in a small amount of PBS on ice. The maxilla and mandible placed in a sterile Petri dish containing sterile Hanks' Balanced Salt Solution (HBSS) on ice were dissected under a stereomicroscope. Surrounding soft tissues were removed, and first molar tooth germs were carefully removed and rinsed in sterile HBSS to eliminate debris while preserving epithelial–mesenchymal integrity.

Trowell-type organ cultures were established by placing tooth germs on mixed cellulose ester membranes (Whatman™, 0.22 μm) supported by stainless steel grids in 60-mm double-well culture dishes (Falcon 353037). Explants were maintained at the air–liquid interface in DMEM supplemented with 100 U/mL penicillin, 100 μg/mL streptomycin, and 100 μg/mL ascorbic acid. Sterile water was added to the outer well to maintain humidity. Medium was changed every other day. Cultures were maintained at 37 °C in 5% CO_2 and examined at 8, 15, 22, and 29 days using a Nikon Eclipse TE300 microscope. Images were captured with a Nikon DXM1200 digital camera.

Results

Cell morphology and GFP reporter expression

Phase-contrast imaging revealed that LS8 cells maintained normal epithelial morphology following transfection, with cell confluency steady increasing from 48 to 96 h post-transfection (Figure 6, A–C). LS8 cells maintained overall epithelial morphology, although an increase in cell debris was observed at 96 h post-transfection.

GFP fluorescence was detectable as early as 48 h after transfection and increased markedly by 72 h, at which time GFP signal intensity and the number of GFP-positive cells were maximum (Figure 6, D–F). By 96 h, GFP fluorescence appeared reduced compared with 72 h, although GFP-positive cells remained detectable. These findings indicate efficient transient expression of the *Slc13a5-GFP* construct, with peak reporter expression occurring at approximately 72 h post-transfection.

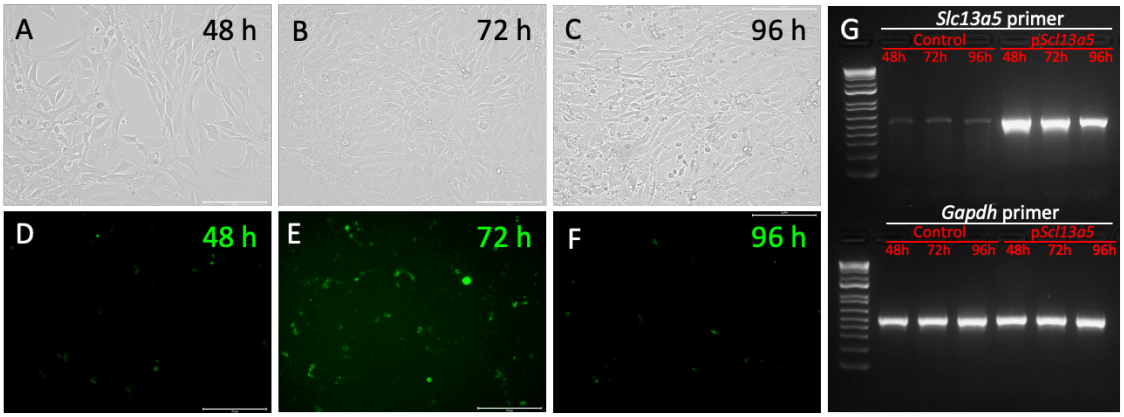


Figure 5: *Slc13a5* overexpression in LS8 cells following plasmid transfection. (A–C) Phase-contrast images showing increasing LS8 cell confluency at 48, 72, and 96 h post-transfection. (D–F) GFP fluorescence images demonstrating peak reporter expression at 72 h. (G, upper) RT-PCR analysis showing *Slc13a5* mRNA expression in transfected cells, with highest expression at 48 h and minimal expression in non-transfected controls. (G, lower) *Gapdh* served as a loading control.

Transcript Analyses

Slc13a5 transcripts were present in LS8 cells at low levels in non-transfected control cells while an increased *Slc13a5* transcripts expression in LS8 cells transfected with the *Slc13a5* plasmid can be detected (Figure 6, G upper). In transfected cells, *Slc13a5* mRNA expression was highest at 48 h post-transfection and gradually decreased at 72 h and 96 h, consistent with transient plasmid-driven expression.

Expression of the housekeeping gene *Gapdh* remained stable across all samples and all time points (Figure 6, G lower), with comparable band intensities observed between control and *Slc13a5*-transfected groups at 48, 72, and 96 h, confirming equal RNA input and reaction consistency.

Immunocytochemistry

To verify successful overexpression of NaCT in LS8 cells, immunocytochemistry was performed 72 hours after transfection with a pCMV6-AC-Slc13a5–GFP plasmid. Cells were stained with an anti-NaCT primary antibody followed by an Alexa Fluor 594–conjugated secondary antibody. Confocal imaging showed that nearly all DAPI-positive nuclei were GFP-positive, indicating high transfection efficiency (Figure 7, GFP-FITC channel). These GFP-positive cells also exhibited cytoplasmic NaCT immunoreactivity in the Texas Red channel, confirming transgene expression and its detection by the antibody.

As expected, non-transfected LS8 cells lacked GFP signal but presented endogenous NaCT immunofluorescence in the Texas Red channel. The merged images clearly distinguish transfected ($GFP^+/NaCT^+$) from non-transfected ($GFP^-/NaCT^+$) populations, demonstrating consistent detection of overexpressed NaCT while also revealing basal endogenous expression within the cell line.

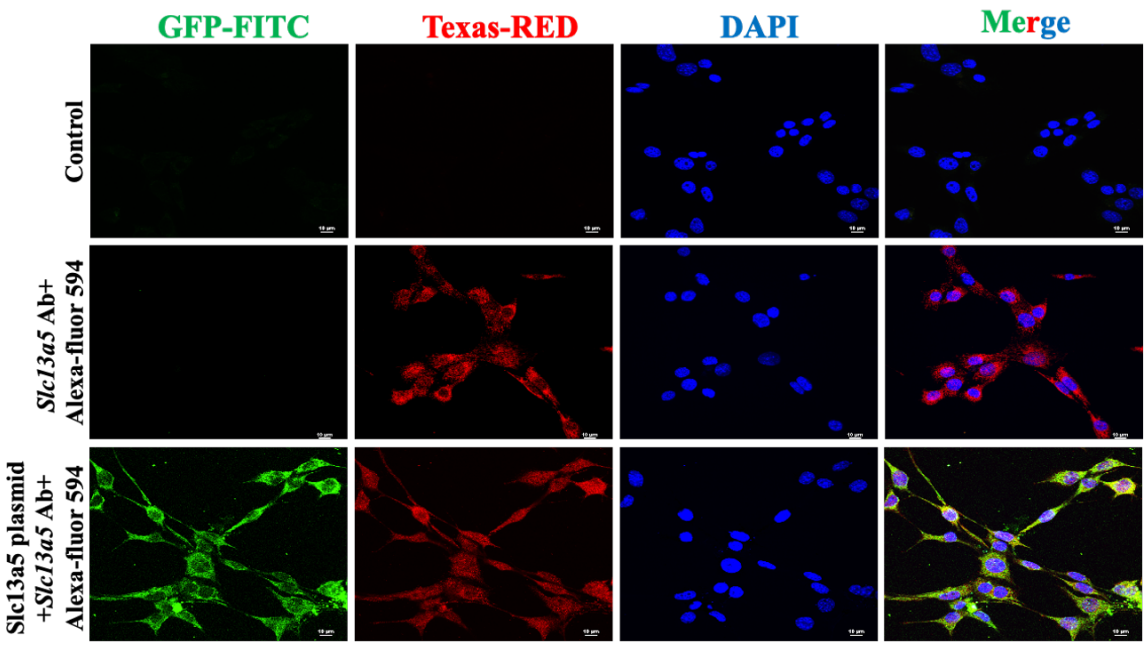


Figure 6: Immunocytochemical detection of Slc13a5 expression in LS8 cells. GFP fluorescence indicates Slc13a5 expressed from the transfected plasmid, whereas red immunofluorescence represents total Slc13a5 protein detected by immunocytochemistry. Non-transfected LS8 cells lacked GFP signal but exhibited detectable endogenous Slc13a5 immunoreactivity. In contrast, GFP-positive cells showed strong cytoplasmic Slc13a5 staining, confirming successful transgene expression.

Tooth Organ Culture

To prepare for gene expression studies in *Slc13a5*$^{R337*/R337*}$ tooth organs, first molar tooth germs from wild-type (WT) and *Slc13a5*$^{R337*/R337*}$ pups were cultured *ex vivo* for up to 29 days. During the culture period, tooth germ explants progressed from the onset of bell stage to the late bell stage by 22 days in culture (Figure 8).

Both WT and *Slc13a5*$^{R337*/R337*}$ tooth germs gradually decreased in size over time, reaching approximately 75% of their initial size by 29 days in culture. However, loss of the epithelial covering occurred earlier in the *Slc13a5*$^{R337*/R337*}$ group than in WT explants which was evident by 15 days. Beginning at 8 days in culture, calcified-like tissue deposits were observed at the cusp tips in both groups. In WT explants, the area of calcified-like tissue expanded gradually and uniformly. In contrast, the deposits in *Slc13a5*$^{R337*/R337*}$ explants appeared irregular in shape and distribution. This observation is consistent with the ectopic mineral nodules identified in histological analyses of the molars from *Slc13a5* null mice.

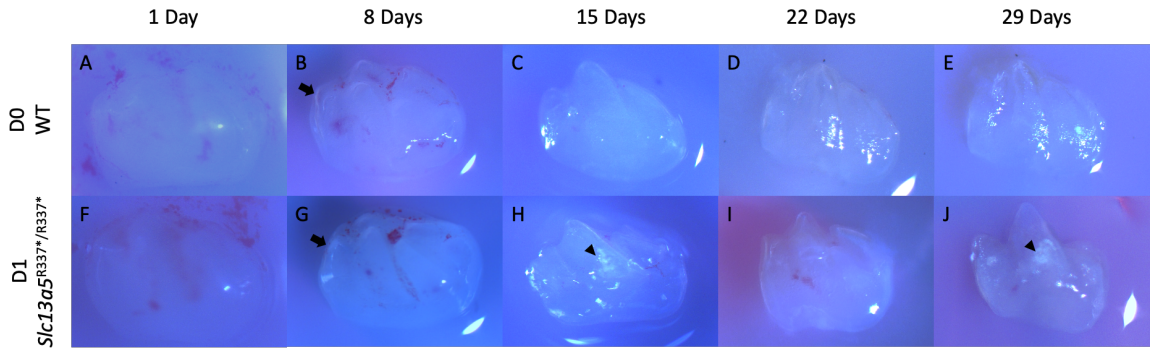


Figure 7: Tooth organ culture of mandibular molars. Mandibular first molar explants cultured for 1, 8, 15, and 22 days (culture day, CD) from postnatal day 0 (D0) wild-type mice (A–E) and postnatal day 1 (D1) *Slc13a5*$^{R337*/R337*}$ mice (F–J). Calcified-like tissue deposits were observed at the cusp tips in both groups (arrows; B, G). In contrast, *Slc13a5*$^{R337*/R337*}$ explants exhibited irregular and heterogeneous calcified-like tissue deposition (arrowheads; H, J).

Discussion

Although DEE25 is primarily characterized as a neurological disorder caused by loss-of-function mutations in *SLC13A5*, affected individuals also exhibit severe enamel defects, particularly hypoplastic amelogenesis imperfecta. These dental abnormalities are clinically visible, noninvasively assessable, and directly reflect impaired NaCT function in mineralizing tissues. In contrast to neurological manifestations, which are complex and difficult to monitor at the cellular level in patients, enamel defects provide a structurally well-defined and experimentally accessible phenotype. Because enamel formation is a tightly regulated developmental process, disruptions in citrate transport can be readily correlated with cellular and extracellular changes in ameloblast behavior and mineral deposition. Therefore, developing tooth organs represents a practical and biologically relevant model for investigating the consequences of NaCT deficiency and offers a measurable platform for evaluating potential therapeutic strategies that may ultimately inform treatment approaches for DEE25.

In the present study, we first established and validated *in vitro* and *ex vivo* systems to support future gene-delivery experiments. In LS8 ameloblast-like cells, plasmid-mediated overexpression successfully increased *Slc13a5* transcript levels and produced detectable NaCT protein, confirming the feasibility of transgene expression and antibody-based detection. The observation that *Slc13a5* mRNA levels peaked earlier than protein expression is consistent with normal gene expression kinetics. Following transfection, transcription occurs rapidly, whereas protein production requires translation, folding, post-translational modification, and intracellular trafficking. These sequential processes introduce a temporal delay between maximal transcript abundance and peak protein detection. Differences in mRNA turnover and protein stability further explain why declining transcript levels do not immediately result in reduced protein levels.

We also observed detectable endogenous NaCT protein in non-transfected LS8 cells despite relatively low transcript levels. This apparent discrepancy likely reflects the longer half-life and accumulation of NaCT protein compared with its mRNA. Basal transcription may be

sufficient to maintain steady-state protein levels. Conversely, although transfected cells exhibited markedly increased *Slc13a5* mRNA expression, protein levels did not increase proportionally. This suggests that protein abundance is regulated by post-transcriptional and post-translational mechanisms, including limitations in translation efficiency, folding capacity, membrane trafficking, and protein stability. These findings highlight the importance of evaluating both transcript and protein levels when assessing gene-delivery efficiency.

The *ex vivo* tooth organ culture system further demonstrated its value as an intermediate model. *Slc13a5*$^{R337*/R337*}$ tooth germs reproduced key phenotypic features observed *in vivo*, including irregular calcified deposits resembling ectopic mineral nodules. This model preserves tooth germ three-dimensional structure and epithelial–mesenchymal interactions while allowing direct manipulation of gene delivery under controlled conditions. Establishing this system provides a critical tool bridging between cell culture studies and *in vivo* experiments. However, the size of the tooth organs decreased over time in our culture sets. Therefore, this system may currently serve primarily as a platform for evaluating short-term construct transfection efficiency. For long-term gene expression and normal tooth germ development, further optimization of this system is required.

Although chemical transfection using Lipofectamine™ 3000 is efficient and convenient for *in vitro* cell culture validation, it produces transient gene expression, as demonstrated by the decline in GFP reporter signal after 72 hours. Such transient expression is insufficient for therapeutic purposes because enamel formation is a prolonged developmental process. In rodents, incisor turnover occurs over approximately one month[14], whereas human molars require several years to complete development[15, 16]. Therefore, a gene-delivery system capable of sustained expression is necessary for meaningful therapeutic intervention.

Moreover, calcification of the permanent dentition begins with the first molars around birth, and first molar crown formation typically requires approximately 30–36 months[16]. This developmental window may represent a critical period for therapeutic intervention in AI. However, delayed tooth eruption has been reported in some *SLC13A5*-associated AI patients[9]. Therefore, the optimal timing for intervention will require further evaluation and may need to be individualized.

Among available gene-delivery approaches, viral vectors offer high transduction efficiency to organs and longer-lasting expression *in vivo*[17]. Adeno-associated virus (AAV)

represents a particularly promising candidate due to its favorable safety profile, low immunogenicity, and rare genomic integration[18]. Importantly, AAV has been successfully applied in multiple FDA-approved gene therapies for inherited disorders, supporting its translational potential[19-21]. In addition, the availability of different AAV serotypes enables tissue-specific targeting, which may allow selective delivery to dental epithelial tissues[22]. Collectively, these features make AAV a strong candidate for future *ex vivo* and *in vivo* rescue experiments in the *Slc13a5*$^{R337*/R337*}$ model.

In vivo experiments are time-consuming, resource-intensive, and require substantial animal use, particularly when assessing developmental outcomes. LS8 cells and *ex vivo* tooth organ cultures provide controlled and efficient systems to optimize construct design, validate expression kinetics, and evaluate preliminary phenotypic effects before advancing to animal studies. Our next step is to generate AAV constructs based on the validated plasmid sequences and test their infection efficiency and gene expression in the established *Slc13a5*$^{R337*/R337*}$ tooth organ model. Successful *ex vivo* validation will provide a strong rationale for subsequent *in vivo* therapeutic studies.

Bibliography

1. Jaramillo-Martinez V, Urbatsch IL, Ganapathy V. Functional Distinction between Human and Mouse Sodium-Coupled Citrate Transporters and Its Biologic Significance: An Attempt for Structural Basis Using a Homology Modeling Approach. Chem Rev 2021;121(9):5359–77.
2. Sauer DB, Song J, Wang B, et al. Structure and inhibition mechanism of the human citrate transporter NaCT. Nature 2021;591(7848):157–61.
3. Granchi D, Baldini N, Ulivieri FM, Caudarella R. Role of Citrate in Pathophysiology and Medical Management of Bone Diseases. Nutrients 2019;11(11).
4. Costello LC, Franklin RB, Reynolds MA, Chellaiah M. The Important Role of Osteoblasts and Citrate Production in Bone Formation: "Osteoblast Citration" as a New Concept for an Old Relationship. Open Bone J 2012;4.
5. Costello LC, Chellaiah M, Zou J, Franklin RB, Reynolds MA. The status of citrate in the hydroxyapatite/collagen complex of bone; and Its role in bone formation. J Regen Med Tissue Eng 2014;3:4.
6. Brown TL, Nye KL, Porter BE. Growth and Overall Health of Patients with SLC13A5 Citrate Transporter Disorder. Metabolites 2021;11(11).
7. Bloch-Zupan A, Rey T, Jimenez-Armijo A, et al. Amelogenesis imperfecta: Next-generation sequencing sheds light on Witkop's classification. Front Physiol 2023;14:1130175.
8. Hardies K, de Kovel CG, Weckhuysen S, et al. Recessive mutations in SLC13A5 result in a loss of citrate transport and cause neonatal epilepsy, developmental delay and teeth hypoplasia. Brain 2015;138(Pt 11):3238–50.
9. Schossig A, Bloch-Zupan A, Lussi A, et al. SLC13A5 is the second gene associated with Kohlschutter-Tonz syndrome. J Med Genet 2017;54(1):54–62.
10. Wright JT. Enamel Phenotypes: Genetic and Environmental Determinants. Genes (Basel) 2023;14(3).
11. Hu JC, Liang T, Zhang H, et al. Citrate Transporter Expression and Localization: The Slc13a5(Flag) Mouse Model. Int J Mol Sci 2025;26(14).
12. Yamada M, Bringas P, Jr., Grodin M, MacDougall M, Slavkin HC. Developmental comparisons of murine secretory amelogenesis in vivo, as xenografts on the chick chorio-allantoic membrane, and in vitro. Calcif Tissue Int 1980;31(2):161–71.
13. Han X, Yoshizaki K, Tian T, et al. Mouse Embryonic Tooth Germ Dissection and Ex vivo Culture Protocol. Bio Protoc 2020;10(3):e3515.
14. Smith CE, Warshawsky H. Cellular renewal in the enamel organ and the odontoblast layer of the rat incisor as followed by radioautography using 3H-thymidine. Anat Rec 1975;183(4):523–61.

15. Dean MC, Cole TJ. Human life history evolution explains dissociation between the timing of tooth eruption and peak rates of root growth. PLoS One 2013;8(1):e54534.
16. Dental Growth and Development. Pediatr Dent 2018;40(6):468.
17. Nayerossadat N, Maedeh T, Ali PA. Viral and nonviral delivery systems for gene delivery. Adv Biomed Res 2012;1:27.
18. Naso MF, Tomkowicz B, Perry WL, Strohl WR. Adeno-Associated Virus (AAV) as a Vector for Gene Therapy. Biodrugs 2017;31(4):317–34.
19. Russell S, Bennett J, Wellman JA, et al. Efficacy and safety of voretigene neparvovec (AAV2-hRPE65v2) in patients with RPE65-mediated inherited retinal dystrophy: a randomised, controlled, open-label, phase 3 trial. Lancet 2017;390(10097):849–60.
20. Mendell JR, Al-Zaidy S, Shell R, et al. Single-Dose Gene-Replacement Therapy for Spinal Muscular Atrophy. New England Journal of Medicine 2017;377(18):1713–22.
21. Pipe SW, Leebeek FWG, Recht M, et al. Gene Therapy with Etranacogene Dezaparvovec for Hemophilia B. New England Journal of Medicine 2023;388(8):706–18.
22. Matsuzaka Y, Yashiro R. Therapeutic Application and Structural Features of Adeno-Associated Virus Vector. Curr Issues Mol Biol 2024;46(8):8464–98.